ChemComm

FEATURE ARTICLE

View Article Online
View Journal | View Issue

Cite this: *Chem. Commun.*, 2026, **62**, 8089

Long-term electrochemical CO_2 reduction *via* electrode regeneration

Guorui Gao, Gelson T. da Silva, Sukhjot Kaur, Hyunwook Kim and Cao-Thang Dinh *

Electrochemical CO_2 reduction (eCO_2RR) offers a direct route to convert waste carbon into fuels and commodity chemicals using renewable electricity, but industrial translation is ultimately constrained by durability under high-rate operation. At practical current densities, performance losses rarely stem from a single failure mode. Instead, catalyst reconstruction and corrosion, impurity-driven poisoning, electrolyte flooding, and carbonate salt precipitation interact to undermine activity, selectivity, and stability. This Feature Article outlines the dominant electrode-level degradation pathways and then critically assesses regeneration strategies that restore performance without replacing electrodes. We review redox-based catalyst reactivation and renewal, hydrophobicity recovery to re-establish stable gas transport pathways, and local-environment reset protocols that dissolve or prevent salt buildup. Together, these approaches reposition regeneration as an integral design standard for long-term CO_2 electrolysis systems compatible with intermittent renewable power.

Received 2nd February 2026,
Accepted 24th March 2026

DOI: 10.1039/d6cc00709k

rsc.li/chemcomm

1. Introduction

Carbon dioxide (CO_2) is the dominant anthropogenic greenhouse-gas contributor and, at the same time, an abundant carbon feedstock for sustainable chemical manufacturing.[1]

Global energy-related CO_2 emissions reached 37.8 Gt in 2024, around 50% higher than in 2000, underscoring the urgency of decarbonization while energy demand continues to grow.[2] Electrochemical CO_2 reduction reaction (eCO_2RR) is attractive because it couples carbon mitigation with energy storage by converting CO_2 into value-added fuels and chemicals using renewable electricity.[3,4] This dual role becomes particularly compelling in energy systems dominated by intermittent

Department of Chemical Engineering, Queen's University, Kingston, ON, K7L 3N6, Canada. E-mail: caothang.dinh@queensu.ca

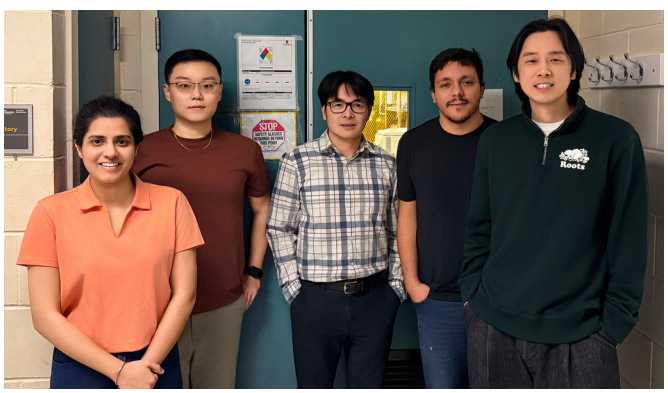

Left to right: Sukhjot Kaur, Guorui Gao, Cao-Thang Dinh, Gelson T. da Silva and Hyunwook Kim

Guorui Gao is a PhD candidate in Prof. Dinh's group at Queen's University. He focuses on developing advanced electrodes and electrolyzers for liquid-fed eCO_2RR. He is broadly interested in electrochemical technologies for the transition toward net-zero carbon emissions.

Gelson Tavares da Silva is a postdoctoral fellow at Queen's University, specializing in the aqueous-fed eCO_2RR systems. With a PhD from UFSCar, he integrates catalyst design and scaling up electrochemical processes for CO_2 conversion and environmental remediation.

Sukhjot Kaur received her PhD in Chemistry from the Indian Institute of Technology Ropar, India, with a focus on electrochemical strategies for mitigating CO_2 and HCl in energy storage and conversion. She is now a postdoctoral fellow in Dinh's Lab, developing electrochemical C–N coupling for highly efficient fertilizer production.

Hyunwook Kim studies electrochemical CO_2 reduction catalysts designed for efficient, long-lasting CO_2 conversion. His research background in porous materials, adsorption, and catalysis has taught him that the most fascinating research areas are rarely the easiest ones.

Cao Thang Dinh is an associate professor of chemical engineering at Queen's University. His research focuses on producing sustainable fuels and chemicals from CO_2, water and renewable electricity.

generation, where chemical products can act as dispatchable energy vectors.

While remarkable advances have been achieved in catalytic activity and selectivity, sustaining these metrics over the long term remains a critical bottleneck to industrial deployment. Techno-economic analyses consistently indicate that practical CO_2 electrolysis requires high faradaic efficiency (FE), low full-cell voltage, and long-term operation at industrially relevant current densities.[5,6] Here, industrially relevant current densities refer broadly to operation at or above $\sim$200 mA cm^{-2}, with several hundred mA cm^{-2} to near-ampere-level current densities often viewed as more commercially meaningful depending on the product and electrolyzer configuration, whereas long-term operation denotes stability over hundreds to thousands of hours in laboratory studies and ultimately multi-year durability at the stack and system levels in practice. Accordingly, the field has shifted from short-term performance benchmarks toward extended testing ($>$1000 h) and accelerated stress protocols designed to reveal the dominant failure modes.[7,8]

Performance decay during high-rate CO_2 electrolysis arises from a combination of catalyst reconstruction and corrosion,[9] electrolyte intrusion and salt accumulation within porous electrodes,[10] and mass-transport instabilities associated with local reaction environment fluctuations.[11] To address this bottleneck, efforts have been directed toward intrinsic stabilization through the development of more robust catalysts[12–14] and gas diffusion electrodes,[15–17] together with improved control over electrolyte composition.[18–20] Such strategies are the preferred first defense because they suppress degradation at its source, but partially reversible decay may still occur under demanding operating conditions. Consequently, periodic regeneration and recovery strategies that restore electrode function without replacing hardware are emerging as an important complement to intrinsic stabilization. In practice, the most effective long-term operating frameworks will likely combine both concepts, where intrinsic stabilization maximizes the operational time between recovery intervention, and regeneration-based approaches extend the overall device lifetime.

In this review, we first summarize electrode-level degradation pathways in state-of-the-art CO_2 electrolyzers and then evaluate regeneration strategies that target distinct failure modes. We classify recovery approaches as redox-mediated catalyst reactivation, wettability and hydrophobicity restoration to recover gas diffusion channels, and local environment reset protocols to maintain three-phase transport. By consolidating a fragmented body of literature, we aim to provide a practical framework for designing durable and recoverable CO_2 electrolysis systems.

2. Electrode degradation mechanisms

The long-term electrochemical CO_2 conversion is highly constrained by electrode degradation, where chemical, electrochemical, and mechanical instabilities operate concurrently. Mechanistic understanding is thus essential for the rational electrode design and for recovery intervention selection. In this section, we categorize electrode degradation into two classes: active catalyst layer and support substrate degradations, respectively. Together, these mechanisms define the overall cathodic durability limitations of high-rate CO_2 electrolyzers.

2.1. Active catalyst degradation

Nanostructured electrocatalysts are inherently dynamic, particularly at high current densities, where interfacial electric fields,[21] local pH gradients,[22] and surface adsorbate coverage[23–27] impose strong thermodynamic and kinetic driving forces for restructuring.[23,28–33] The reconstruction can result in the loss of high-index facets and undercoordinated sites, nanoparticle growth or agglomerations, and collapse of nanostructured architectures, ultimately shifting product selectivity and compromising long-term stability. Structural and phase evolution under eCO_2RR conditions is often described as an early stage dominated by particle migration and coalescence, followed by Ostwald ripening during prolonged operation (Fig. 1a).[34]

A first transition commonly occurs during the electroreduction of oxide or hydroxide precursors. For example, metastable copper (Cu) oxides/hydroxides can be rapidly converted into nanocrystalline metallic Cu during start-up (Fig. 1b), yielding metallic Cu as the persistent phase under extended eCO_2RR operations.[35] Beyond this initial transition, Cu catalysts continue to undergo pronounced reaction-driven reconstruction. Operando studies, assisted by theoretical analyses, have shown that *CO intermediates can form mobile Cu–carbonyl (Cu–CO) species, enabling surface atom migration and transforming shape-controlled nanocubes into polycrystalline nanograins.[36] Complementarily, other pathways invoke reactive oxygen-containing species generated *in situ* (*e.g.*, OH radicals) that stabilize $Cu^{\delta+}$ motifs and promote fragmentation, migration, and anisotropic growth into high-curvature structures.[37]

Over longer operation, reconstruction can be further accelerated by oxidation–reduction cycling and by dissolution–redeposition processes, rather than proceeding solely through direct solid-state rearrangement.[34,38] In other words, catalyst restructuring does not always occur only by atom migration within the solid electrode; under reaction conditions, part of the catalyst can transiently dissolve into the interfacial environment and then redeposit, producing a continuously evolving surface. As an illustrative case for Cu catalysts (Fig. 1c), cathodic operation can generate transient Cu^+ species at the bulk catalyst surface, which may coordinate with adsorbed intermediates to form soluble Cu-containing complexes such as $[CuCO]^+$.[39] These intermediates allow Cu atoms to temporarily leave the original lattice before being reduced and redeposited as metallic Cu under cathodic bias, thereby continuously renewing surface morphology. Beyond *CO- and oxide-mediated pathways, alkali-cation-assisted cathodic corrosion has also been identified at sufficiently negative potentials, where cations facilitate the extraction of Cu atoms through transient soluble intermediates, leading to progressive roughening and particle fragmentation.[40]

In parallel with intrinsic reconstruction, extrinsic impurities can impose substantial performance penalties.[41–45] Trace metallic

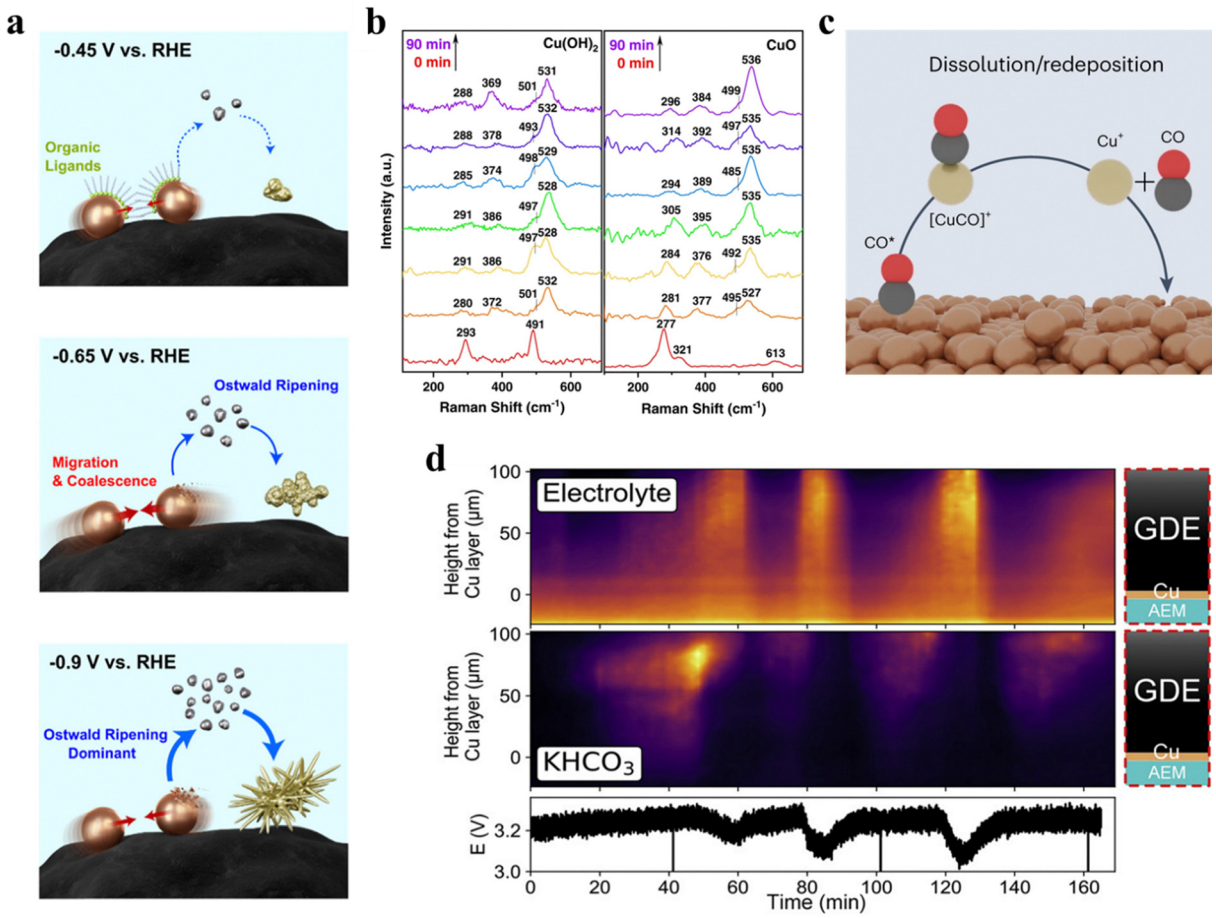

Fig. 1 Typical electrode degradation mechanisms for active catalyst layer and support substrate degradations. (a) Schematic illustration of the structural transformation of CuO_x NPs during eCO_2RR as a function of applied potential. Adapted with permission.[34] Copyright 2025, The Authors, American Chemical Society. (b) Time-resolved operando Raman spectra images of $Cu(OH)_2$ (left) and CuO nanocrystals (right) at their optimum potential for C_{2+} production during eCO_2RR. Adapted with permission.[35] Copyright 2022, The Authors, Springer Nature. (c) Schematic illustration of the copper reconstruction under eCO_2RR conditions. Reprinted with permission.[39] Copyright 2024, Springer Nature. (d) Evolution of electrolyte content and salt precipitates in the GDE over electrolysis time at 100 mA cm^{-2}. Reprinted with permission.[61] Copyright 2023, The Authors, Elsevier.

contaminants in electrolytes, such as Fe, Ni, or Zn, may deposit on Cu under cathodic bias, modify adsorption energetics, and promote hydrogen evolution, causing apparent selectivity decay that originates from surface poisoning rather than structural collapse.[42] Similarly, contaminants in flue gas-derived CO_2 streams can disperse current through competing reduction pathways. For instance, oxygen and nitrogen oxides typically suppress eCO_2RR transiently *via* oxygen reduction or nitrate/nitrite reduction,[46,47] whereas sulfur-containing impurities (*e.g.*, SO_2) can cause more persistent deactivation through sulfur incorporation and irreversible changes in surface composition and product distribution.[48,49]

2.2. Support substrate degradation

In addition to catalyst stability, the porous electrode architecture strongly influences durability, particularly in CO_2 gas-fed configurations, where stable gas diffusion pathways are essential. Here, performance losses frequently arise from electrolyte flooding and (bi)carbonate salt accumulation, which reduce effective mass transport and impose local reactant starvation even when the catalyst itself remains active.

Salt precipitation is tightly linked to local alkalization.[50–55] During CO_2 electrolysis, hydroxide ions generated at the cathode react with CO_2 to form (bi)carbonate species, which subsequently pair with alkali cations to generate soluble salts. At high current densities, local supersaturation promotes crystallization within the catalyst layer and gas diffusion layer (GDL). In parallel, liquid products and electro-wetting reduce the local contact angle, enabling electrolyte intrusion into pores.[56] Hydrophilic salt crystallites then nucleate along pore walls and progressively weaken hydrophobicity, creating a feedback loop that accelerates flooding and further promotes precipitation.

The net effects of salt crystallization and electrolyte intrusion are pore blockage, restricted gas transport, and CO_2 depletion at active sites, leading to a selectivity shift toward hydrogen evolution (HER) and a sharp decrease in CO_2 utilization.[57–60] An operando structural probe has directly

visualized the progressive electrolyte invasion and salt formation inside gas diffusion electrodes (Fig. 1d), highlighting that support failure can dominate performance decay even when the catalyst surface chemistry remains largely unchanged.[61]

Severe salt buildup can also trigger mechanical damage, including structural deformation, catalyst-layer delamination, and loss of electrical contact.[62,63] In membrane electrode assembly (MEA) setups, deposits at the membrane–electrode interface increase ionic resistance and exacerbate voltage losses.[61] Mechanical stresses from pressure fluctuations, such as gas bubble detachment, further contribute to particle loss and thinning of weakly adhered catalyst layers,[64–66] while long-term polarization can degrade binders and induce pore collapse or stress fatigue in carbon-paper and foam substrates.[67–69]

Overall, electrode degradation during eCO_2RR reflects the coupled evolution of catalyst state, wetting, and local chemistry. These coupled failure modes explain why durability cannot be addressed by catalyst design alone. Importantly, many of these processes are partially reversible or kinetically controllable, providing a rationale for regeneration strategies that restore function *in situ* and extend device lifetime without full electrode replacement. Instead, practical CO_2 electrolyzers will likely rely on a combination of materials that tolerate reconstruction, and operating protocols that periodically restore the electrode and interfacial environment before irreversible damage accumulates.

3. Electrode regeneration

Since high-rate eCO_2RR performance decay often originates from changes in catalyst state, electrode wettability, and interfacial ion chemistry, regeneration has emerged as a pragmatic route to sustain operation when electrode replacement is economically or operationally infeasible. This section summarizes representative approaches for catalyst reactivation, hydrophobicity recovery, and local environment resetting that enable extended electrolyzer lifetimes without system interruption.

3.1. Active catalyst regeneration

Even well-designed catalysts typically exhibit an early performance maximum followed by a gradual selectivity drift. Given that practical deployment requires operation over decades,[4] *in situ* regeneration protocols based on controlled chemical or electrochemical redox provide an appealing alternative to frequent catalyst replacement.[70,71] Pulsed-operation approaches are one important practice in which the applied current or potential is intentionally modulated over time, rather than maintained at a constant steady-state cathodic bias.[72] These protocols can involve brief anodic pulses, open-circuit or rest intervals, or other programmed current/potential waveforms inserted into cathodic operation. The underlying concept is that these transient steps can partially reset the evolving electrode interface during operation by partially restoring catalyst surface states or active-site accessibility and removing accumulated surface species. Pulsed operation is therefore increasingly considered not only to influence instantaneous selectivity, but also to slow degradation and regenerate electrode performance during extended CO_2 electrolysis.

An illustrative approach from our previous work is periodic *in situ* chemical oxidation (Fig. 2a–c), in which brief exposure of the Cu cathode to an oxidizing environment restores catalytic activity without disassembling the reactor.[73] In an on/off regeneration protocol, alternating oxidative treatment (15 min at open circuit voltage) and eCO_2RR operation (15 min) periodically re-oxidizes reconstructed Cu surfaces and renews catalytic function, maintaining ethylene (C_2H_4) FE of at least 40% with stable cell voltage for over 200 h (Fig. 2a). Notably, aggressive anodic pulsing (*e.g.*, 5 s at 0.5 mA cm^{-2}) instead of chemical oxidation produced less stable operation dominated by overall catalyst morphology change and salt precipitation, suggesting that slow, spontaneous oxidation can simultaneously recover catalyst state while limiting (bi)carbonate accumulation.

Programmable electrochemical oxidation offers precise control over regeneration intensity and frequency. By tuning the anodic charge during pulsed CO_2 electrolysis, we revealed that the Cu oxidation state (Cu^+/Cu^{2+}) can be modulated to sustain selectivity and mitigate irreversible reconstruction (Fig. 2d).[74] We found that both the oxidation current density and durability critically influence product selectivity and catalyst stability. A brief and mild oxidative pulse (1 mA cm^{-2} for 24 s) enabled a Cu gas diffusion electrode (GDE) to maintain high C_2H_4 selectivity above 50% for approximately 120 h at 150 mA cm^{-2}, compared with only around 5 h under continuous operation. Moreover, we extended similar redox-based recovery to Sn-based electrodes, achieving stable formate ($HCOO^-$) production with 90% FE for more than 160 h at 100 mA cm^{-2}, emphasizing the broad applicability of electrochemical regeneration.[76]

Beyond reactivating an existing catalyst layer, recoverable operation can be viewed as a specific, programmed form of regeneration in which catalyst formation and deactivation are treated as controllable and reversible steps within a single device. Rather than restoring a partially degraded catalyst, this approach periodically resets the active phases through *in situ* cyclic catalyst fabrication and removal during operation (Fig. 2e). In bicarbonate-fed systems, we demonstrated that active Cu sites can be periodically generated by electrodeposition of metal–ligand precursors from the catholyte along with CO_2 electrolysis, followed by electro-oxidation to dissolve deactivated species and refresh the substrate surface.[75] Using this concept, sustained CO_2-to-CH_4 conversion with over 60% faradaic efficiency was achieved for more than 500 h at current densities above 0.2 A cm^{-2}. Importantly, the same strategy enabled cumulative operation beyond 100 days under day-on/night-off cycling (Fig. 2f), illustrating a practical match to intermittent renewable electricity.

Taken together, redox-mediated regeneration and recoverable operation provide operational methods to reverse deactivation and extend catalyst lifetime. Rather than considering catalyst evolution as purely detrimental, these studies demonstrate that programmable state control can be integrated into electrolyzer operation to sustain high-rate CO_2 conversion.

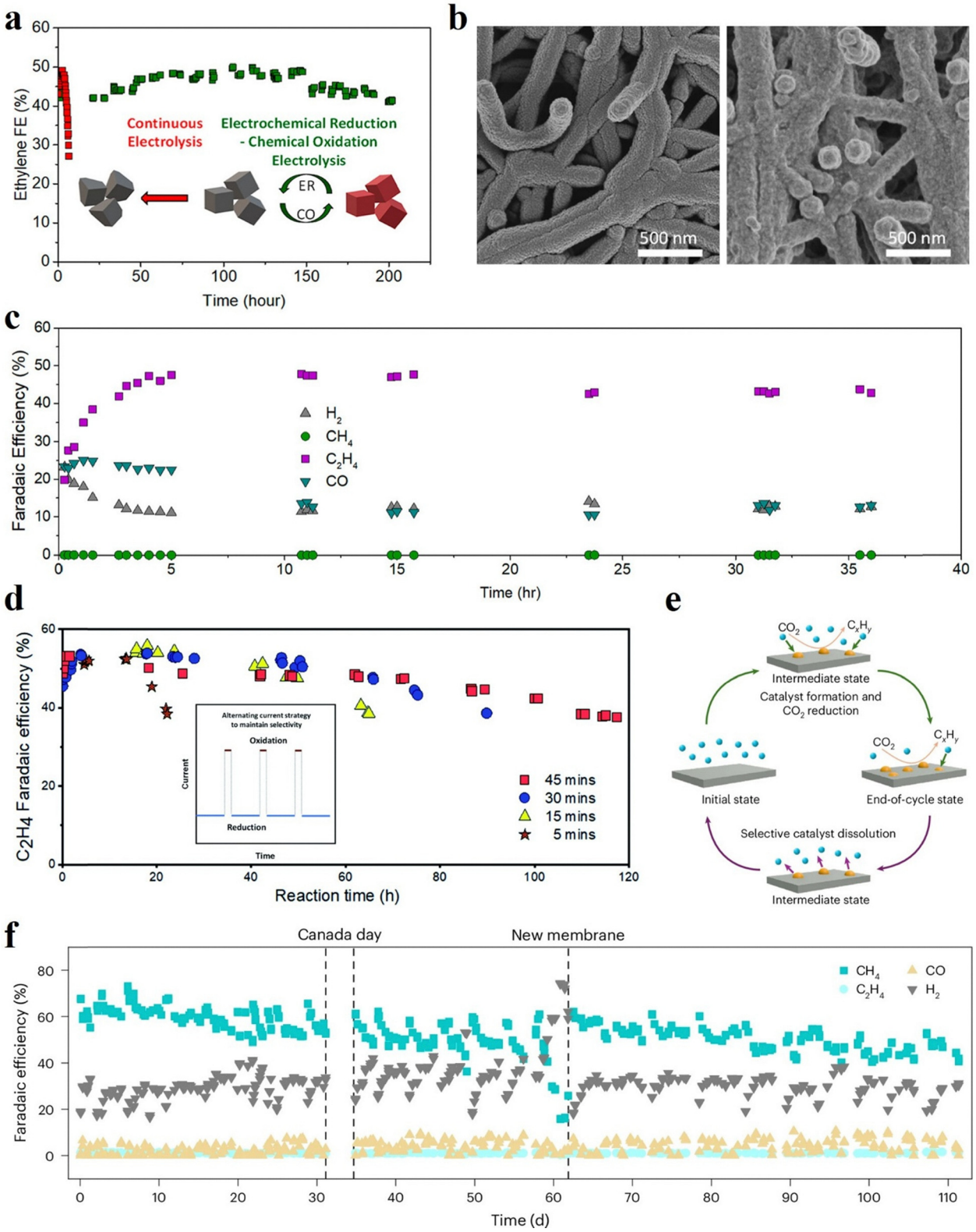

Fig. 2 *In situ* active catalyst regeneration strategies to sustain active catalytic sites during CO_2 electrolysis. (a) Stability comparison of C_2H_4 FE between continuous electrolysis and pulsed electrolysis using alternating electrochemical reduction and chemical oxidation segments over a Cu/PTFE GDE at the cathodic current density of 150 mA cm^{-2}, (b) SEM images of Cu/PTFE before (left) and after (right) 200 h of "on" time electrolysis, and (c) catalyst regeneration for 1 A cm^{-2} density operation, with continuous electrolysis for 5 h followed by pulsed electrolysis of alternating-/15 min "on"/15 min "off"/-segments. Only the "on" time is shown. Reprinted with permission.[73] Copyright 2022, American Chemical Society. (d) Stability of Cu/PTFE GDE under electrochemical reduction/oxidation segments with different reduction times at 150 mA cm^{-2} and a fixed oxidation current density and time of 1 mA cm^{-2} and 24 s, respectively. The schematic illustration of the alternating current strategy is inserted. Reprinted with permission.[74] Copyright 2022, Royal Society of Chemistry. (e) "Recoverable operation" approach on *in situ* prepared Cu catalysts, and (f) intermittent operation of the system with alternating 12-hour on/12-hour off and recoverable operation strategy. Reprinted with permission.[75] Copyright 2025, The Authors, Springer Nature.

3.2. Hydrophobicity regeneration

Durable CO_2 electrolysis requires not only stable active sites but also persistent gas access to the catalyst layer.[57,61] In GDE architecture, hydrophobic GDL suppresses electrolyte intrusion and enables efficient CO_2 transport, yet prolonged polarization can gradually ruin the interfacial hydrophobicity and trigger flooding. Wettability-oriented regeneration, therefore, aims to restore gas transport pathways without necessarily altering catalyst composition.

An illustrative example employs CuO nanoelectrodes functionalized with 1-dodecanethiol (DDT), where the hydrophobic DDT coating stabilizes the interfacial structure and improves CO_2 access, thereby enhancing eCO_2RR performance (Fig. 3a).[77] During extended electrolysis, performance decay was attributed to gradual thiol loss caused by oxidative transformation, resulting in a quantified 17.3% reduction in DDT coverage. Periodic *ex situ* DDT re-treatment restored surface thiol coverage and recovered C_2H_4 FE, which remained a FE of 52.1% after 160 h (Fig. 3b). More broadly, periodic *ex situ* reprocessing of GDE with polytetrafluoroethylene (PTFE) emulsion (every 200 h) has enabled stable CO_2-to-formic acid operation for up to 5200 h (Fig. 3c) by mitigating electrowetting at the three-phase interface (Fig. 3d).[8]

However, these examples should be viewed as representative demonstrations rather than universally deployable regeneration protocols, particularly for continuous-flow systems. Specifically, many current regeneration protocols that require *ex situ* handling or dedicated bypass operations can introduce downtime and added process complexity, making uninterrupted operation difficult. More broadly, the practical deployment of chemical regeneration strategies in flow cells or stack-relevant configurations is constrained not only by treatment effectiveness, but also by hardware compatibility. Any such protocol must remain compatible with the full MEA, including membranes, ionomers, and sealing components, to avoid chemical contamination, unwanted interfacial damage, or other integration-related problems.

Operational strategies, most notably pulsed protocols, can also mitigate or even reverse flooding tendencies without physically reprocessing the electrode. For instance, pulsed electrolysis has been shown to sustain multicarbon production at industrially relevant current densities (>0.2 A cm^{-2}) primarily by suppressing flood-assisted mass-transport losses rather than by inducing persistent catalyst restructuring.[58] By periodically restoring the electrolyte contact angle on GDE and stabilizing the gas–liquid interface, pulsed operation can retard salt-assisted electrolyte intrusion into the GDE and reduce HER under high current densities.

Although the strategies discussed above directly focus on hydrophobicity recovery, electrode architecture and system-level design can reduce the need for regeneration. In this context, Fang *et al.* engineered a carbon-based GDL by coating an insulating yet highly hydrophobic PTFE matrix, reinforced with a sparse conductive carbon nanotube network, into which Cu nanoparticles were further embedded (Fig. 3e).[59] This hydrophobic and selectively conductive architecture suppresses electric-field-driven cation accumulation for (bi)carbonate crystallization while maintaining efficient electron and CO_2 transport. By confining locally generated OH^- for C–C coupling, the design enabled stable C_2H_4 production for over 1000 h (Fig. 3f). Complementarily, a hydrophobic coating on the gas flow channel with parylene can promote drainage of salt-containing electrolyte droplets before drying out (Fig. 3g), thereby suppressing local salt crust formation on flow channels.[60] This system-level modification resulted in a five-fold enhancement in operational stability (500 h) for carbon monoxide (CO) production (Fig. 3h).

Overall, hydrophobic engineering across both electrodes and flow fields can effectively suppress flooding and salt accumulation, reducing the reliance on active regeneration strategies. While electrode reprocessing and pulsed-operation approaches provide effective near-term means to sustain performance, the long-term objective is to embed hydrophobic resilience directly into electrode and system designs, so that regeneration becomes the exception rather than the norm.

3.3. Local reaction regeneration

Salt precipitation represents a major durability challenge in gas-fed CO_2 electrolysis, particularly under alkaline conditions and high current densities, where local ion concentrations and pH gradients can become extreme. Salt deposits obstruct gas transport pathways, reduce effective active catalytic areas, and accelerate performance decay, motivating strategies that either prevent supersaturation or actively dissolve deposits during operation.[78]

In MEA reactors operated with alkaline anolytes, one mitigation route is to limit alkali–cation crossover. Replacing alkaline anolyte with pure water can suppress cation transport to the cathode and reduce (bi)carbonate precipitation, while periodic infusion of cation-containing solutions from the GDE backside to the catalyst layer can transiently restore local alkali cation concentration on the catalyst surface to maintain eCO_2RR activity when needed.[79]

Gas management provides another handle. Humidified CO_2 feeding can delay salt formation by maintaining water balance. There is one study elucidating that no precipitates were observed during 120 min operation at 150 mA cm^{-2} under humidification, whereas salt deposits formed over similar time scales without humidification, even at 100 mA cm^{-2}.[80] However, at higher current densities where humidification alone becomes insufficient, trace addition of volatile acid vapors to the CO_2 feed has been demonstrated to remove deposits from the cathode chamber and gas flow channels (Fig. 4a), enabling stable CO_2-to-CO electrolysis for up to 4500 h (Fig. 4b).[81]

Electrochemical self-cleaning through potential modulation has also proven effective. A voltage-pulsing protocol that alternates between a high operational cathodic voltage (60 s) and a lower regeneration cathodic voltage (30 s) can drive electromigration of accumulated ions away from the cathode, reduce local supersaturation, and preserve gas pathways (Fig. 4d).[82] Using this strategy, stable ethylene production was sustained for an efficient time of 157 h (Fig. 4e), whereas continuous

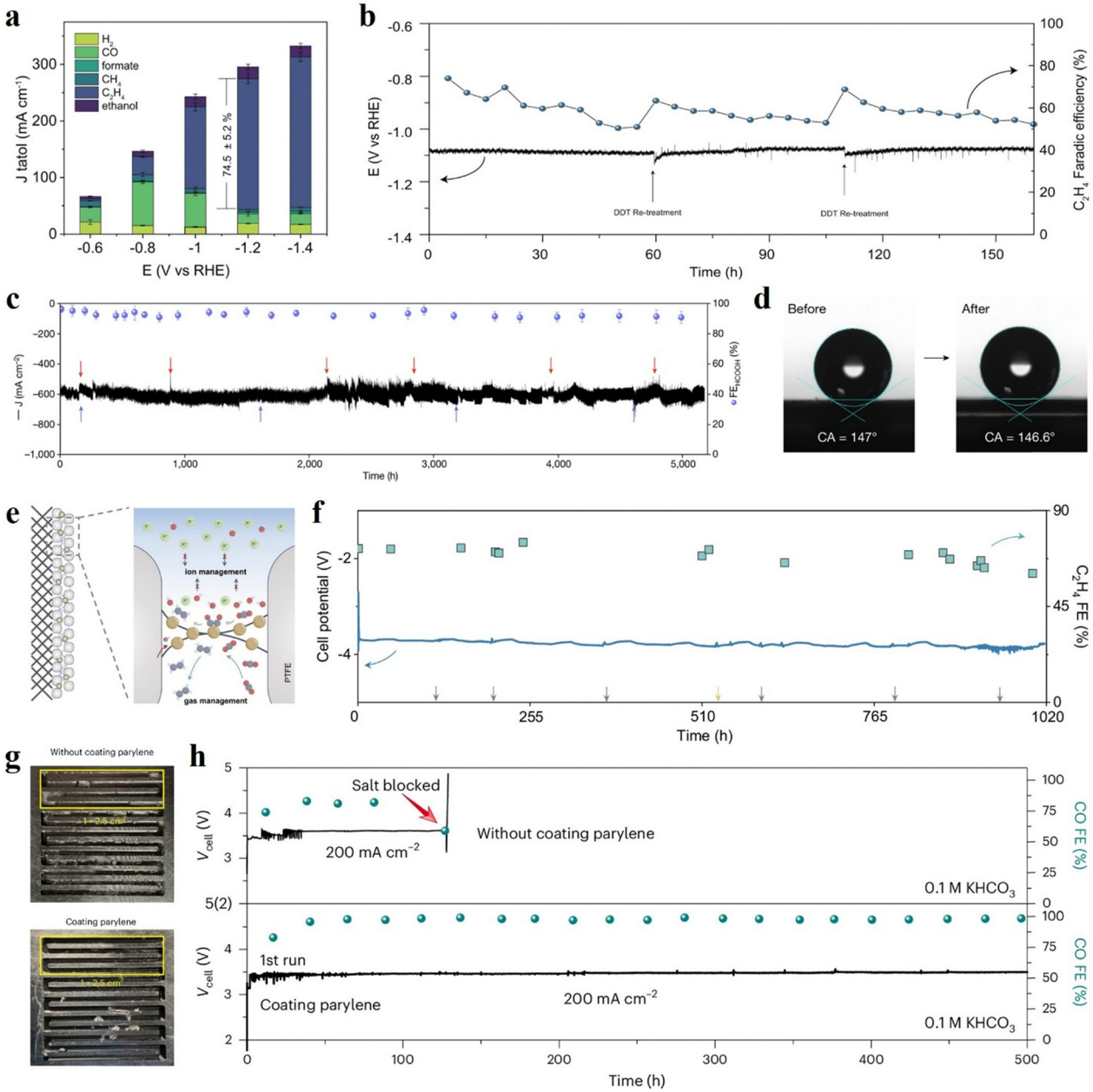

Fig. 3 Hydrophobicity regeneration strategies for GDEs to sustain gas transport pathways during CO_2 electrolysis. (a) Current densities and product distributions at different potentials over DDT functionalized CuO electrode under flow cell measurement, and (b) long-term CO_2 electrolysis with periodic *ex situ* DDT re-treatment restores the hydrophobicity of the electrode and C_2H_4 selectivity. Reprinted with permission.[77] Copyright 2024, The Authors, Springer Nature. (c) Electrochemical stability at a cell voltage of 2.2 V with a periodic *ex situ* hydrophobicity regeneration strategy, where red and blue arrows represent replacement of electrolyte and reaction gas, respectively, and (d) representative static water contact angle images of the GDE before and after stability test, indicating that periodic *ex situ* reprocessing with a polytetrafluoroethylene emulsion preserves high hydrophobicity. Reprinted with permission.[8] Copyright 2024, Springer Nature. (e) Schematic of Cu catalyst embedded in a PTFE/CNT matrix, and (f) eCO_2RR stability of the electrode operated at 200 mA cm^{-2} in a MEA electrolyzer (full-cell potentials without iR correction). Gray and yellow arrows indicate the time points when the electrolyte and the anion exchange membrane were refreshed, respectively. Reprinted with permission. (ref. 59) Copyright 2025, The Authors, Springer Nature. (g) Photographs of the distribution of $KHCO_3$ in the pristine cathode flow channels *versus* parylene-coated cathode metal plate after the control test at 100 mA cm^{-2} using 0.5 M $KHCO_3$ after 10 h, and (h) stabilities of Ag-based electrode at 200 mA cm^{-2} using 0.1 M $KHCO_3$ anolyte in MEA electrolyzer with pristine cathode flow channels *versus* parylene-coated cathode flow channels. Reprinted with permission.[60] Copyright 2025, Springer Nature.

operation failed within approximately 10 h due to rapid salt accumulation (Fig. 4c).

As coupled with pulsed operation, membrane properties become equally critical in mitigating salt precipitation. We demonstrated an ambipolar ion transport membrane (AITM)-assisted gas-diffusion MEA system that suppresses salt accumulation by allowing simultaneous transport of anions, cations, and water to maintain a stable pH gradient across

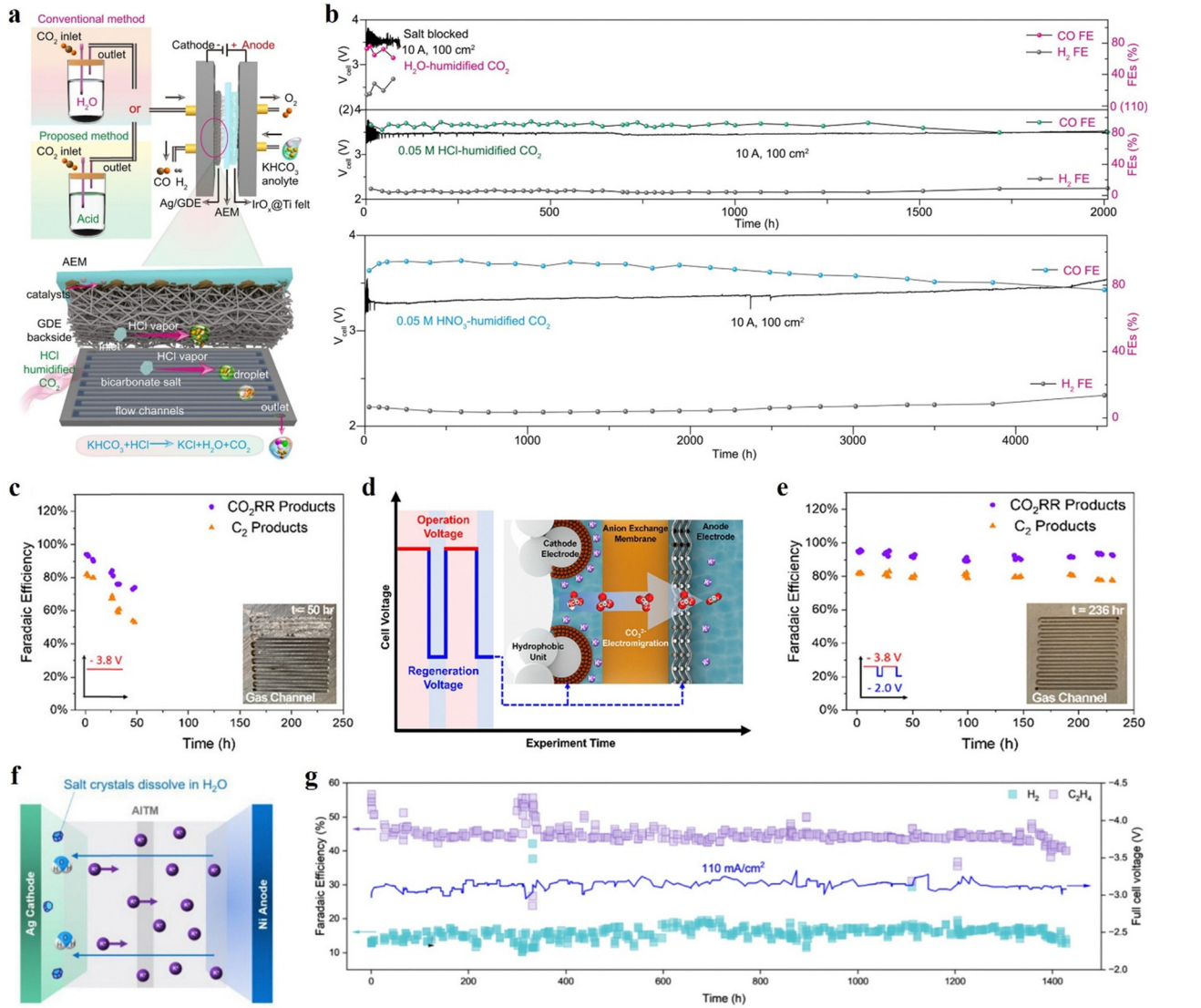

Fig. 4 Local reaction environment regeneration to sustain a stable and favorable microenvironment of triple-phase boundary during CO_2 electrolysis. (a) Schematic representation of a conventional eCO_2RR MEA electrolyzer using H_2O-humidified *versus* acid-humidified CO_2, and (b) stability tests of the 100 cm^2 eCO_2RR MEA at 100 mA cm^{-2}, with 200 sccm of H_2O-humidified CO_2 *versus* 0.05 M HCl- and 0.05 M HNO_3-humidified CO_2. Reprinted with permission.[81] Copyright 2025, American Association for the Advancement of Science. (c) Selectivity of continuously operating Cu/PTFE at −3.8 V during long-term operation, (d) the strategy to mitigate carbonate formation by cycling between operational and regeneration cell voltages, and (e) the corresponding electrochemical performance under optimal alternating conditions for long-term operation. Reprinted with permission.[82] Copyright 2021, American Chemical Society. (f) Salt accumulated during eCO_2RR is dissolved back into the solution from the anolyte during the off-cycle of the on/off cycling strategy, and (g) FEs of gas products and cell voltage in the stability tests at 110 mA cm^{-2} in the AITM system using 1 M $KHCO_3$ anolyte and Ni anode (the total "on time" is 950 h). Reprinted with permission.[83] Copyright 2025, The Authors, Wiley.

electrodes, even with concentrated anolytes. Integrated with alternating on/off operation for *in situ* catalyst recovery, the high-water permeability of the AITM promotes dissolution of precipitated carbonate salts during off cycles, effectively resetting the local reaction environment without catalyst replacement (Fig. 4f). This approach enabled stable noble-metal-free CO_2 electrolysis for >950 h (total "on" time) at 110 mA cm^{-2} and a cell voltage of 3.15 V (Fig. 4g), underscoring regeneration approaches that rely on ion and water management rather than active site reconstruction alone.[83]

It is worth noting that periodic regeneration or pulsed operation introduces brief non-productive intervals and therefore imposes an additional energy penalty. However, this penalty can remain small because recovery pulses are often short and applied at low current. For instance, the self-cleaning CO_2 electrolyzer[82] discussed above required <1% additional energy input for regeneration while extending stable high-rate C_2 production from <10 h to >150 h. Similarly, in our "recoverable operation strategy",[75] the anodic regeneration step contributed a <1% charge penalty relative to the overall redox process. In parallel, techno-economic analysis[84] suggests that, under favorable duty-cycle and FE conditions, pulsed operation can even reduce the minimum selling price of ethylene relative to steady-state operation. Together, these examples show that

the overall impact of pulsing is system-dependent and can be beneficial when improvements in selectivity and durability outweigh the added recovery cost.

In summary, local environment reset strategies based on electrolyte selection, feedstock management, pulse control, and membrane design provide viable pathways to suppress salt precipitation and extend high-rate operation. These concepts are most effective when integrated with catalyst and hydrophobicity regeneration, reflecting the coupled nature of electrode degradation.

4. Conclusion and outlook

Electrode degradation remains the central obstacle to translating high-rate eCO_2RR from laboratory demonstrations to industrial operation. Catalyst reconstruction, impurity-driven deactivation, and support-level flooding/salt precipitation jointly deteriorate performance and, importantly, can reinforce one another. The body of work reviewed here demonstrates that regeneration can interrupt these degradation pathways, as controlled oxidative treatments and pulsed waveforms can recover catalyst surfaces, hydrophobicity restoration can refresh gas transport pathways, and local environment reset approaches can dissolve or prevent carbonate accumulation. Achieving industrially relevant lifetimes will therefore require tight integration of materials design with operational control. Regeneration strategies further emphasize that durability is not solely a materials-selection challenge, since many failure modes can be slowed, reversed, or periodically reset by tuning redox state, wettability, and ion and water fluxes. Table 1 summarizes the performance of the proposed electrode regeneration strategies in this review.

Future opportunities in electrode regeneration for eCO_2RR should move beyond isolated recovery of individual degradation modes toward more integrated and predictive design frameworks. At the materials and interface level, this includes developing catalysts, substrates, and interfacial layers that can tolerate repeated redox cycling without cumulative damage. More importantly, regeneration strategies should increasingly address multiple degradation dimensions simultaneously, rather than focusing on only one aspect at a time. In practice, this means coupling active-site renewal with local-environment refreshing and restoration of substrate or interfacial functionalization, so that catalyst deactivation, salt accumulation, and loss of hydrophobicity can be managed in a coordinated manner. In parallel, regeneration should shift from a predominantly post-failure recovery concept toward preventive control, in which intervention occurs before severe performance loss accumulates. This will require pulsed or other programmed recovery protocols that minimize energy penalties while maximizing restoration of catalytic activity, transport pathways, and interfacial stability.

Equally important, electrode regeneration must be evaluated at the full-device level rather than only by its local recovery effect. A practically useful regeneration strategy should not restore one system component at the expense of another. In other words, regeneration protocols should not accelerate membrane degradation, ionomer damage, interfacial delamination, or other unwanted component deterioration. As the field moves closer to industrial deployment, regeneration strategies must also be tested under more realistic feed conditions, including impurity-containing CO_2 streams or electrolyte precursors, where degradation may arise not only from intrinsic catalyst evolution but also from impurity-derived contamination.

Another major direction is the compatibility of regeneration with large-scale or stack-level systems. Although pilot-scale systems and stacks have made substantial progress toward continuous CO_2 electrolysis, translating regeneration-based strategies to these platforms introduces additional system-level constraints beyond those observed in single-cell studies. In particular, pulsed or periodic operation can create spatially heterogeneous environments across large electrode areas, making uniform current and potential distribution especially significant. Regeneration protocols, such as on–off or oxidation–reduction pulses, must therefore be carefully tailored to avoid

Table 1 Comparison of performance metrics across different electrode regeneration strategies

Cathode	Electrolyzer	Product	CD* (mA cm^{-2})	FE (%)	Stability* (h)	Strategy
Cu/PTFE	Flow cell	C_2H_4	150	~50 to ~41	200	*In situ* P-CO*[73]
Cu NPs-Cu/PTFE	Flow cell	C_2H_4	1000	~48 to ~43	31	*In situ* P-CO*[73]
Cu/PTFE	Flow cell	C_2H_4	150	~53 to ~37	~120	*In situ* P-EO*[74]
Sn/Ag/PTFE	Flow cell	$HCOO^-$	100	~92 to ~90	~160	*In situ* P-EO*[76]
Cu/Ag mesh	MEA cell	CH_4	>200	>60	~500	*In situ* RO*[75]
CuO–SH GDE	Flow cell	C_2H_4	200	~74 to ~52	~165	*Ex situ* P-HR*[77]
r-Pb GDE	Flow cell	HCOOH	~600	~98 to ~91	5200	*Ex situ* P-HR*[8]
Cu/carbon fiber	Flow cell	C_2H_4	~750	~40 to ~37	2.5	Pulsed electrolysis[58]
Cu–PC/carbon fiber	Flow cell	C_2H_4	200	~80 to ~60	1020	Hydrophobicity reinforcement[59]
Ag NPs/carbon paper	MEA cell	CO	200	>90	500	Flow channel pre-HT*[60]
Ag NPs/carbon paper	MEA cell	CO	420 ± 50	~90	~220	Periodic infusion[79]
Ag NPs/carbon paper	MEA cell	CO	100	~90 to ~80	~4500	Acid humidification[81]
Cu/Ag NPs/carbon paper	MEA cell	C_{2+}	120–250	~82 to ~77	236	Pulsed electrolysis[82]
Cu/PTFE	MEA cell	C_2H_4	110–147	~55 to ~40	1400	Pulsed electrolysis[83]

Note: CD*: current density; Stability* includes both operation and regeneration time; P-CO*: periodic chemical oxidation; P-EO*: periodic electrochemical oxidation; RO*: recoverable operation; P-HR*: periodic hydrophobicity regeneration; Pre-HT*: pre-hydrophobicity treatment.

localized overstress and accelerated degradation in specific electrode regions. At the stack level, they must also preserve cell-to-cell uniformity in mass transport and operating conditions. Consequently, regeneration steps should avoid large voltage transients, minimize added complexity in electrolyte and flow management, and remain compatible with standard stack hardware, control logic, and maintenance schedules. Protocols that leverage natural downtime (*e.g.*, renewable intermittency, planned maintenance intervals) may offer an efficient pathway to extend lifetime without sacrificing effective operation time. These considerations suggest that the industrial feasibility of regeneration will depend not only on the reversibility of degradation chemistry, but also on whether recovery protocols can be integrated into continuous operation in a scalable, energy-efficient, and operationally robust manner.

From a system perspective, coupling electrode regeneration with sensing and feedback control is a particularly compelling research trend. Real-time indicators such as local ion concentration, heat distribution, product selectivity drift, or local impedance can be used to trigger targeted system recovery only when and where it is needed, thereby reducing unnecessary efficiency losses. Ultimately, the long-term goal is to embed electrode regeneration as a planned and adaptive operating mode, rather than a corrective measure. In this sense, the future of electrode regeneration in CO_2 electrolyzers will likely lie in preventive, multi-dimensional, device-compatible, and control-integrated strategies that are designed not only to restore performance, but also to sustain stable operation under realistic and scalable conditions.

Author contributions

This article was prepared with joint contributions from all authors.

Conflicts of interest

There are no conflicts to declare.

Data availability

No primary research results, software or code have been included, and no new data were generated or analyzed as part of this article.

Acknowledgements

The authors acknowledge financial support from the Natural Sciences and Engineering Research Council of Canada (NSERC), TOTALEnergies, and Queen's University.

References

1 R. G. Grim, Z. Huang, M. T. Guarnieri, J. R. Ferrell, L. Tao and J. A. Schaidle, *Energy Environ. Sci.*, 2020, **13**, 472–494.
2 G. C. B. (2025), – with major processing by Our World in Data, https://ourworldindata.org/co2-emissions (accessed January 21, 2026).
3 R. Daiyan, I. MacGill and R. Amal, *ACS Energy Lett.*, 2020, **5**, 3843–3847.
4 P. De Luna, C. Hahn, D. Higgins, S. A. Jaffer, T. F. Jaramillo and E. H. Sargent, *Science*, 2019, **364**, eaav3506.
5 B. Belsa, L. Xia and F. P. García de Arquer, *ACS Energy Lett.*, 2024, **9**, 4293–4305.
6 H. S. Moon, S. A. Jaffer, R. K. Miao, E. H. Sargent and D. Sinton, *Nat. Rev. Mater.*, 2026, **11**, 244–254.
7 U. O. Nwabara, M. P. de Heer, E. R. Cofell, S. Verma, E. Negro and P. J. A. Kenis, *J. Mater. Chem. A*, 2020, **8**, 22557–22571.
8 W. Fang, W. Guo, R. Lu, Y. Yan, X. Liu, D. Wu, F. M. Li, Y. Zhou, C. He, C. Xia, H. Niu, S. Wang, Y. Liu, Y. Mao, C. Zhang, B. You, Y. Pang, L. Duan, X. Yang, F. Song, T. Zhai, G. Wang, X. Guo, B. Tan, T. Yao, Z. Wang and B. Y. Xia, *Nat.*, 2024, **626**, 86–91.
9 J. Huang, N. Hörmann, E. Oveisi, A. Loiudice, G. L. De Gregorio, O. Andreussi, N. Marzari and R. Buonsanti, *Nat. Commun.*, 2018, **9**, 3117.
10 J. Biemolt, J. Singh, G. Prats Vergel, H. M. Pelzer and T. Burdyny, *ACS Energy Lett.*, 2025, **10**, 807–814.
11 B. Nourmohammadi Khiarak, G. T. S. T. da Silva, V. Grange, G. Gao, V. Golovanova, F. P. de García de Arquer, L. H. Mascaro and C.-T. Dinh, *Small*, 2025, **21**, 2409669.
12 V. Okatenko, A. Loiudice, M. A. Newton, D. C. Stoian, A. Blokhina, A. N. Chen, K. Rossi and R. Buonsanti, *J. Am. Chem. Soc.*, 2023, **145**, 5370–5383.
13 Z. Li, P. Wang, X. Lyu, V. K. R. Kondapalli, S. Xiang, J. D. Jimenez, L. Ma, T. Ito, T. Zhang, J. Raj, Y. Fang, Y. Bai, J. Li, A. Serov, V. Shanov, A. I. Frenkel, S. D. Senanayake, S. Yang, T. P. Senftle and J. Wu, *Nat. Chem. Eng.*, 2024, **1**, 159–169.
14 T. Zheng, K. Jiang, N. Ta, Y. Hu, J. Zeng, J. Liu and H. Wang, *Joule*, 2019, **3**, 265–278.
15 H. Noh, H. Yeo, B. W. Boudouris and B. M. Tackett, *Energy Environ. Sci.*, 2025, **18**, 1272–1281.
16 M. Sun, J. Cheng and M. Yamauchi, *Nat. Commun.*, 2024, **15**, 491.
17 C.-T. Dinh, T. Burdyny, M. G. Kibria, A. Seifitokaldani, C. M. Gabardo, F. P. García de Arquer, A. Kiani, J. P. Edwards, P. De Luna, O. S. Bushuyev, C. Zou, R. Quintero-Bermudez, Y. Pang, D. Sinton and E. H. Sargent, *Science*, 2018, **360**, 783–787.
18 Y. Chen, J. A. Wrubel, A. E. Vise, F. Intia, S. Harshberger, E. Klein, W. A. Smith, Z. Ma, T. G. Deutsch and K. C. Neyerlin, *Chem Catal.*, 2022, **2**, 400–421.
19 J. E. Huang, F. Li, A. Ozden, A. Sedighian Rasouli, F. P. García de Arquer, S. Liu, S. Zhang, M. Luo, X. Wang, Y. Lum, Y. Xu, K. Bertens, R. K. Miao, C.-T. Dinh, D. Sinton and E. H. Sargent, *Science*, 2021, **372**, 1074–1078.
20 G. Marcandalli, M. C. O. Monteiro, A. Goyal and M. T. M. Koper, *Acc. Chem. Res.*, 2022, **55**, 1900–1911.
21 R. Yang, Y. Cai, Y. Qi, Z. Tang, J.-J. Zhu, J. Li, W. Zhu and Z. Chen, *Nat. Commun.*, 2024, **15**, 7140.
22 H. Liu, T. Yan, S. Tan, L. Sun, Z. Zhang, S. Hu, S.-H. Li, X. Kang, Y. Lei, L. Jiang, T. Hou, L. Liu, Q. Yu and B. Liu, *J. Am. Chem. Soc.*, 2024, **146**, 5333–5342.
23 S. Zhang, Q. Tang, B. Zhu and Y. Gao, *ACS Catal.*, 2025, **15**, 6497–6506.
24 J. Zhu, J. Li, R. Lu, R. Yu, S. Zhao, C. Li, L. Lv, L. Xia, X. Chen, W. Cai, J. Meng, W. Zhang, X. Pan, X. Hong, Y. Dai, Y. Mao, J. Li, L. Zhou, G. He, Q. Pang, Y. Zhao, C. Xia, Z. Wang, L. Dai and L. Mai, *Nat. Commun.*, 2023, **14**, 4670.
25 R. Amirbeigiarab, J. Tian, A. Herzog, C. Qiu, A. Bergmann, B. Roldan Cuenya and O. M. Magnussen, *Nat. Catal.*, 2023, **6**, 837–846.
26 A. S. Varela, W. Ju, T. Reier and P. Strasser, *ACS Catal.*, 2016, **6**, 2136–2144.
27 D. Cheng, K.-L. C. Nguyen, V. Sumaria, Z. Wei, Z. Zhang, W. Gee, Y. Li, C. G. Morales-Guio, M. Heyde, B. Roldan Cuenya, A. N. Alexandrova and P. Sautet, *Nat. Commun.*, 2025, **16**, 4064.
28 X. Ma, T. Yang, D. He, X. Gao, W. Jiang, D. Li, Y. Sun, X. Lin, J. Xu, H. Wang, X. Tai, Y. Lin, T. Yao, H. Zhou and Y. Wu, *Nat. Synth.*, 2025, **4**, 53–66.
29 J. Kok, P. P. Albertini, J. Leemans, R. Buonsanti and T. Burdyny, *Nat. Rev. Mater.*, 2025, **10**, 550–563.
30 C. Han, V. Kundi, Z. Ma, C. Y. Toe, P. Kumar, C. Tsounis, J. Jiang, S. Xi, Z. Han, X. Lu, R. Amal and J. Pan, *Adv. Funct. Mater.*, 2023, **33**, 2210938.

31 C. Long, X. Liu, K. Wan, Y. Jiang, P. An, C. Yang, G. Wu, W. Wang, J. Guo, L. Li, K. Pang, Q. Li, C. Cui, S. Liu, T. Tan and Z. Tang, *Science Adv.*, 2023, **9**, eadi6119.
32 Y. Jiang, X. Wang, D. Duan, C. He, J. Ma, W. Zhang, H. Liu, R. Long, Z. Li, T. Kong, X. J. Loh, L. Song, E. Ye and Y. Xiong, *Adv. Sci.*, 2022, **9**, 2105292.
33 X. Ren, F. Liu, H. Wu, Q. Lu, J. Zhao, Y. Liu, J. Zhang, J. Mao, J. Wang, X. Han, Y. Deng and W. Hu, *Angew. Chem. Int. Ed.*, 2024, **63**, e202316640.
34 S. H. Lee, J. E. Avilés Acosta, D. Lee, D. M. Larson, H. Li, J. Chen, J. Lee, E. Erdem, D. U. Lee, S. J. Blair, A. Gallo, H. Zheng, A. C. Nielander, C. J. Tassone, T. F. Jaramillo and W. S. Drisdell, *J. Am. Chem. Soc.*, 2025, **147**, 6536–6548.
35 Q. Lei, L. Huang, J. Yin, B. Davaasuren, Y. Yuan, X. Dong, Z.-P. Wu, X. Wang, K. X. Yao, X. Lu and Y. Han, *Nat. Commun.*, 2022, **13**, 4857.
36 Y. Yang, J. Feijóo, M. Figueras-Valls, C. Chen, C. Shi, M. V. Fonseca Guzman, Y. Murhabazi Maombi, S. Liu, P. Jain, V. Briega-Martos, Z. Peng, Y. Shan, G. Lee, M. Rebarchik, L. Xu, C. J. Pollock, J. Jin, N. E. Soland, C. Wang, M. B. Salmeron, Z. Chen, Y. Han, M. Mavrikakis and P. Yang, *Nat. Catal.*, 2025, **8**, 579–594.
37 L. Wang, Z. Chen, Y. Xiao, L. Huang, X. Wang, H. Fruehwald, D. Akhmetzyanov, M. Hanson, Z. Chen, N. Chen, B. Billinghurst, R. D. L. Smith, C. V. Singh, Z. Tan and Y. A. Wu, *Nat. Commun.*, 2024, **15**, 7477.
38 D. Takamatsu, N. Fukatani, A. Yoneyama, T. Hirano, K. Hirai, S. Yabuuchi, K. Watanabe, K. Kamiya and S. Nakanishi, *J. Am. Chem. Soc.*, 2025, **147**, 24103–24112.
39 J. Vavra, G. P. L. Ramona, F. Dattila, A. Kormányos, T. Priamushko, P. P. Albertini, A. Loiudice, S. Cherevko, N. Lopéz and R. Buonsanti, *Nat. Catal.*, 2024, **7**, 89–97.
40 S. Liu, Y. Li, D. Wang, S. Xi, H. Xu, Y. Wang, X. Li, W. Zang, W. Liu, M. Su, K. Yan, A. C. Nielander, A. B. Wong, J. Lu, T. F. Jaramillo, L. Wang, P. Canepa and Q. He, *Nat. Commun.*, 2024, **15**, 5080.
41 Z. Cui, M. A. Marx, M. N. Tegomoh and A. C. Co, *ACS Energy Lett.*, 2023, **8**, 5201–5205.
42 J. He, A. Huang, N. J. J. Johnson, K. E. Dettelbach, D. M. Weekes, Y. Cao and C. P. Berlinguette, *Inorg. Chem.*, 2018, **57**, 14624–14631.
43 Z. P. Jovanov, J. Ferreira de Araujo, S. Li and P. Strasser, *J. Phys. Chem. C*, 2019, **123**, 2165–2174.
44 A. F. Staerz, M. van Leeuwen, T. Priamushko, T. Saatkamp, B. Endrődi, N. Plankensteiner, M. Jobbagy, S. Pahlavan, M. J. W. Blom, C. Janáky, S. Cherevko and P. M. Vereecken, *Angew. Chem., Int. Ed.*, 2024, **63**, e202306503.
45 A. Wuttig and Y. Surendranath, *ACS Catal.*, 2015, **5**, 4479–4484.
46 S. Van Daele, L. Hintjens, S. Hoekx, B. Bohlen, S. Neukermans, N. Daems, J. Hereijgers and T. Breugelmans, *Appl. Catal., B*, 2024, **341**, 123345.
47 D. J. D. Pimlott, A. Jewlal, B. A. W. Mowbray and C. P. Berlinguette, *ACS Energy Lett.*, 2023, **8**, 1779–1784.
48 W. Luc, B. H. Ko, S. Kattel, S. Li, D. Su, J. G. Chen and F. Jiao, *J. Am. Chem. Soc.*, 2019, **141**, 9902–9909.
49 D. Tian, Q. Wang, Z. Qu and H. Zhang, *Nano Energy*, 2025, **134**, 110563.
50 Y. Wu, L. Charlesworth, I. Maglaya, M. N. Idros, M. Li, T. Burdyny, G. Wang and T. E. Rufford, *ACS Energy Lett.*, 2022, **7**, 2884–2892.
51 Y. Kong, H. Hu, M. Liu, Y. Hou, V. Kolivoška, S. Vesztergom and P. Broekmann, *J. Catal.*, 2022, **408**, 1–8.
52 M. Wrobel, S. Kriescher, T. Schiffer, R. Keller and M. Wessling, *Chem. Eng. J.*, 2023, **474**, 145335.
53 F. Bernasconi, A. Senocrate, P. Kraus and C. Battaglia, *EES Catal.*, 2023, **1**, 1009–1016.
54 L. Li, J. Chen, V. S. S. Mosali, Y. Liang, A. M. Bond, Q. Gu and J. Zhang, *Angew. Chem. Int. Ed.*, 2022, **61**, e202208534.
55 L. Li, X. Zhang, C. Liu, V. S. S. Mosali, J. Chen, A. M. Bond, Q. Gu and J. Zhang, *Appl. Catal., B*, 2023, **331**, 122597.
56 C. P. O'Brien, D. McLaughlin, T. Böhm, Y. C. Xiao, J. P. Edwards, C. M. Gabardo, M. Bierling, J. Wicks, A. Sedighian Rasouli, J. Abed, D. Young, C.-T. Dinh, E. H. Sargent, S. Thiele and D. Sinton, *Joule*, 2024, **8**, 2903–2919.
57 Y.-J. Ko, C. Lim, J. Jin, M. G. Kim, J. Y. Lee, T.-Y. Seong, K.-Y. Lee, B. K. Min, J.-Y. Choi, T. Noh, G. W. Hwang, W. H. Lee and H.-S. Oh, *Nat. Commun.*, 2024, **15**, 3356.
58 J. Lin, K. Li, Y. Ye, M. Lu, G. Zhao, P. Xu and L. Chen, *Angew. Chem., Int. Ed.*, 2026, **65**(5), e21745.
59 M. Fang, Z. Huang, M. Wang, Z. Wang, X. Feng, J. Ma, L. Dai, Y. Zhu and L. Jiang, *Nat. Commun.*, 2026, **17**, 984.
60 S. Hao, A. Elgazzar, N. Ravi, T.-U. Wi, P. Zhu, Y. Feng, Y. Xia, F.-Y. Chen, X. Shan and H. Wang, *Nat. Energy*, 2025, **10**, 266–277.
61 A. B. Moss, S. Garg, M. Mirolo, C. A. Giron Rodriguez, R. Ilvonen, I. Chorkendorff, J. Drnec and B. Seger, *Joule*, 2023, **7**, 350–365.
62 S. A. Lee, M. J. Jang, Z. Qi, K. Wang, I. Sullivan, L. Paradis-Fortin, D. Y. Parkinson, W. S. Drisdell, H. A. Atwater and C. Xiang, *EES Catal.*, 2025, **3**, 1302–1314.
63 L. Xu, P. Trogadas, Y. Lan, S. Jiang, S. Zhou, F. Iacoviello, W. Du, R. Jervis and M.-O. Coppens, *ACS Energy Lett.*, 2025, **10**, 3081–3088.
64 R. Fischer, M. A. Dessiex, F. Marone and F. N. Büchi, *ACS Appl. Energy Mater.*, 2024, **7**, 3590–3601.
65 R. Fischer, M. A. Dessiex, L. Gubler, S. Haussener and F. N. Büchi, *J. Mater. Chem. A*, 2025, **13**, 33924–33934.
66 N. Todoroki, K. Nagasawa, H. Enjoji and S. Mitsushima, *ACS Appl. Mater. Interfaces*, 2023, **15**, 24399–24407.
67 U. O. Nwabara, A. D. Hernandez, D. A. Henckel, X. Chen, E. R. Cofell, M. P. de-Heer, S. Verma, A. A. Gewirth and P. J. A. Kenis, *ACS Appl. Energy Mater.*, 2021, **4**, 5175–5186.
68 U. O. Nwabara, E. R. Cofell, S. Verma, E. Negro and P. J. A. Kenis, *ChemSusChem*, 2020, **13**, 855–875.
69 I. V. Zenyuk, D. Y. Parkinson, L. G. Connolly and A. Z. Weber, *J. Power Sources*, 2016, **328**, 364–376.
70 J. Kok, J. de Ruiter, W. van der Stam and T. Burdyny, *J. Am. Chem. Soc.*, 2024, **146**, 19509–19520.
71 K. Ye, T.-W. Jiang, H. D. Jung, P. Shen, S. M. Jang, Z. Weng, S. Back, W.-B. Cai and K. Jiang, *Nat. Commun.*, 2024, **15**, 9781.
72 C. A. Obasanjo, G. Gao, B. N. Khiarak, T. H. Pham, J. Crane and C.-T. Dinh, *Energy Fuels*, 2023, **37**, 13601–13623.
73 T. N. Nguyen, Z. Chen, A. S. Zeraati, H. S. Shiran, S. M. Sadaf, M. G. Kibria, E. H. Sargent and C.-T. Dinh, *J. Am. Chem. Soc.*, 2022, **144**, 13254–13265.
74 C. A. Obasanjo, A. S. Zeraati, H. S. Shiran, T. N. Nguyen, S. M. Sadaf, M. G. Kibria and C.-T. Dinh, *J. Mater. Chem. A*, 2022, **10**, 20059–20070.
75 G. Gao, B. N. Khiarak, H. Liu, T. Trân-Phú, C. A. Obasanjo, J. Crane, H. D. T. Lai, G. T. S. T. da Silva, V. Golovanova, J. Li, H. Ze, J. Weiss, Z. Zhang, S. Lee, R. K. Hocking, F. P. García de Arquer, E. H. Sargent and C.-T. Dinh, *Nat. Energy*, 2025, **10**, 1360–1370.
76 B. N. Khiarak, A. Fell, N. Anand, S. M. Sadaf and C.-T. Dinh, *Catal. Today*, 2024, **426**, 114393.
77 Y. Yao, T. Shi, W. Chen, J. Wu, Y. Fan, Y. Liu, L. Cao and Z. Chen, *Nat. Commun.*, 2024, **15**, 1257.
78 M. Sassenburg, M. Kelly, S. Subramanian, W. A. Smith and T. Burdyny, *ACS Energy Lett.*, 2023, **8**, 321–331.
79 B. Endrődi, A. Samu, E. Kecsenovity, T. Halmágyi, D. Sebők and C. Janáky, *Nat. Energy*, 2021, **6**, 439–448.
80 D. G. Wheeler, B. A. W. Mowbray, A. Reyes, F. Habibzadeh, J. He and C. P. Berlinguette, *Energy Environ. Sci.*, 2020, **13**, 5126–5134.
81 S. Hao, A. Elgazzar, S.-K. Zhang, T.-U. Wi, F.-Y. Chen, Y. Feng, P. Zhu and H. Wang, *Science*, 2025, **388**, eadr3834.
82 Y. Xu, J. P. Edwards, S. Liu, R. K. Miao, J. E. Huang, C. M. Gabardo, C. P. O'Brien, J. Li, E. H. Sargent and D. Sinton, *ACS Energy Lett.*, 2021, **6**, 809–815.
83 T. H. Pham, H. D. T. Lai, N. K. Dang, T. N. Nguyen, V. Golovanova, E. H. Dias, A.-D. Ho, L. Xia, J. Crane, F. P. G. de Arquer, E. H. Sargent, D. Sinton and C.-T. Dinh, *Adv. Energy Mater.*, 2025, **15**, e04286.
84 Y. L. Chung, S. Kim, Y. Lee, D. T. Wijaya, C. W. Lee, K. Jin and J. Na, *iScience*, 2024, **27**, 110383.